Cell Reports

Article

Mutations that adapt SARS-CoV-2 to mink or ferret do not increase fitness in the human airway

Graphical abstract

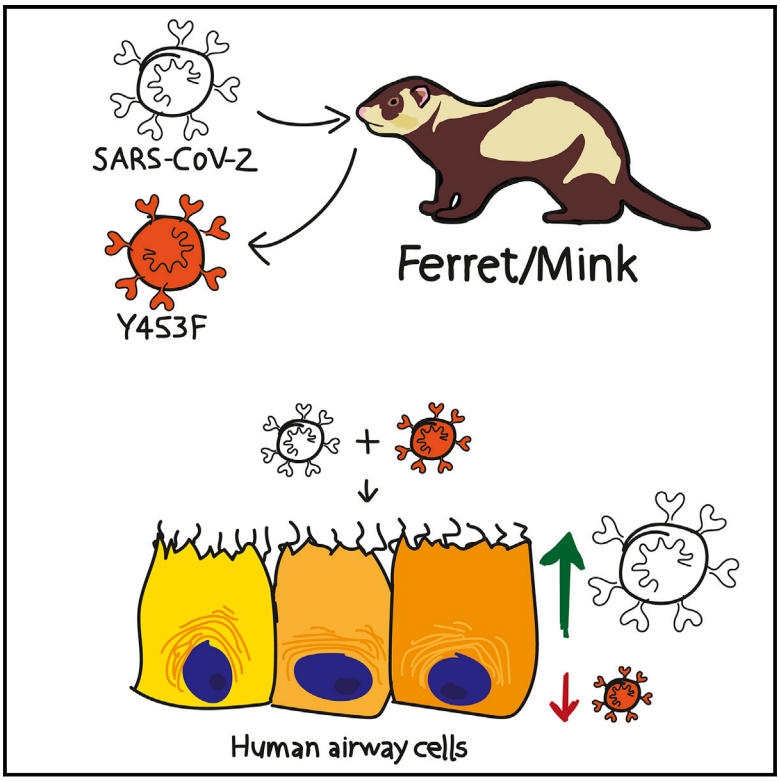

Highlights

- Y453F, F486L, and N501T often arise in SARS-CoV-2 spike during ferret/mink adaptation
- These mutations specifically adapt SARS-CoV-2 to use ferret ACE2
- Common ferret or mink adaptations attenuate the virus in human airway cells
- SARS-CoV-2 variants can use ferret ACE2 with any adaptation

Authors

Jie Zhou, Thomas P. Peacock, Jonathan C. Brown, ..., Julian A. Hiscox, Dalan Bailey, Wendy S. Barclay

Correspondence

w.barclay@imperial.ac.uk

In brief

Zhou et al. show that common mink/ferret adaptations of SARS-CoV-2 enhance the use of the otherwise poorly used ferret ACE2 receptor, while weakening virus replication in human airway cells. However, many SARS-CoV-2 variants can intrinsically enter cells via ferret ACE2 implying these hosts may be more susceptible to novel strains.

Zhou et al., 2022, Cell Reports *38*, 110344
February 8, 2022
https://doi.org/10.1016/j.celrep.2022.110344

CellPress

Cell Reports

CellPress
OPEN ACCESS

Article

Mutations that adapt SARS-CoV-2 to mink or ferret do not increase fitness in the human airway

Jie Zhou,[1,8] Thomas P. Peacock,[1,8] Jonathan C. Brown,[1,8] Daniel H. Goldhill,[1,8] Ahmed M.E. Elrefaey,[2] Rebekah Penrice-Randal,[3] Vanessa M. Cowton,[4] Giuditta De Lorenzo,[4] Wilhelm Furnon,[4] William T. Harvey,[4] Ruthiran Kugathasan,[1] Rebecca Frise,[1] Laury Baillon,[1] Ria Lassaunière,[5] Nazia Thakur,[2,6] Giulia Gallo,[2] Hannah Goldswain,[3] I'ah Donovan-Banfield,[3] Xiaofeng Dong,[3] Nadine P. Randle,[3] Fiachra Sweeney,[1] Martha C. Glynn,[1] Jessica L. Quantrill,[1] Paul F. McKay,[1] Arvind H. Patel,[4] Massimo Palmarini,[4] Julian A. Hiscox,[3,7] Dalan Bailey,[2] and Wendy S. Barclay[1,9,*]

[1]Department of Infectious Disease, Imperial College London, London, UK
[2]The Pirbright Institute, Woking, Surrey, UK
[3]Institute of Infection, Veterinary and Ecology Sciences, University of Liverpool, Liverpool, UK
[4]MRC-University of Glasgow Centre for Virus Research, Glasgow, UK
[5]Virus & Microbiological Special Diagnostics, Statens Serum Institut, Copenhagen, Denmark
[6]The Jenner Institute, Nuffield Department of Medicine, University of Oxford, Oxford, UK
[7]Infectious Diseases Horizontal Technology Centre (ID HTC), A*STAR, Singapore, Singapore
[8]These authors contributed equally
[9]Lead contact
*Correspondence: w.barclay@imperial.ac.uk
https://doi.org/10.1016/j.celrep.2022.110344

SUMMARY

SARS-CoV-2 has a broad mammalian species tropism infecting humans, cats, dogs, and farmed mink. Since the start of the 2019 pandemic, several reverse zoonotic outbreaks of SARS-CoV-2 have occurred in mink, one of which reinfected humans and caused a cluster of infections in Denmark. Here we investigate the molecular basis of mink and ferret adaptation and demonstrate the spike mutations Y453F, F486L, and N501T all specifically adapt SARS-CoV-2 to use mustelid ACE2. Furthermore, we risk assess these mutations and conclude mink-adapted viruses are unlikely to pose an increased threat to humans, as Y453F attenuates the virus replication in human cells and all three mink adaptations have minimal antigenic impact. Finally, we show that certain SARS-CoV-2 variants emerging from circulation in humans may naturally have a greater propensity to infect mustelid hosts and therefore these species should continue to be surveyed for reverse zoonotic infections.

INTRODUCTION

Severe acute respiratory syndrome coronavirus 2 (SARS-CoV-2) is a betacoronavirus that is thought to have emerged from an animal source in 2019 and rapidly spread by human-to-human transmission across the globe causing the coronavirus disease 2019 (COVID-19) pandemic. SARS-CoV-2 is transmitted efficiently by the airborne route due to its ability to efficiently enter cells in the upper respiratory tract. The spike glycoprotein is responsible for host receptor binding and membrane fusion of coronaviruses. SARS-CoV-2 spike binds to host angiotensin-converting enzyme 2 (ACE2) via the receptor binding domain (RBD) and is activated by TMPRSS2 protease expressed at the apical surface of the airway epithelium to mediate fusion (Hoffmann et al., 2020b). In addition, compared with closely related coronaviruses, SARS-CoV-2 spike contains a tract of basic amino acids at the S1/S2 cleavage site that can be recognized by furin, enabling spike to be efficiently primed for fusion by TMPRSS2. This allows rapid fusion of spike at the cell surface and avoids restriction factors present in the late endosome and endolysosome (Hoffmann et al., 2020a; Peacock et al., 2021a).

A series of molecular interactions between amino acids in the spike RBD and the interacting surface of ACE2 result in SARS-CoV-2 binding to human ACE2 with high affinity (Conceicao et al., 2020; Yan et al., 2020). SARS-CoV-2 shows a broad host tropism and can experimentally infect many animal species, largely determined by the efficiency with which spike can interact with the animal ACE2 orthologues (Conceicao et al., 2020; Zhao et al., 2020). For example, mice are inefficiently infected by early SARS-CoV-2 isolates unless they are engineered to transgenically express human ACE2, or SARS-CoV-2 is adapted to murine ACE2 by serial mouse passage (Gu et al., 2020; Rathnasinghe et al., 2021).

From April 2020, reverse zoonotic outbreaks (i.e., transmitted from humans into animals; also known as zooanthroponosis) of

SARS-CoV-2 in mink farms were reported in the Netherlands, the United States, France, Spain, Denmark, Italy, Sweden, Canada, Greece, Lithuania, and Poland (Hammer et al., 2021; Lu et al., 2021; OIE, 2021; Oude Munnink et al., 2020; Rabalski et al., 2021). Multiple reverse zoonotic events introduced the virus from farm workers into densely populated farms that then supported rapid transmission between animals (Hammer et al., 2021; Oude Munnink et al., 2020). Sequence analyses revealed several mutations in spike enriched after circulation in mink, most commonly the amino acid substitutions Y453F or N501T; residues that map to the RBD of spike protein (Hammer et al., 2021; Lu et al., 2021; Oude Munnink et al., 2020). From June to November 2020, an outbreak of SARS-CoV-2 infections occurred among farmed mink in Denmark, with continuous spillover to farm workers and local communities with viruses harboring Y453F (Hammer et al., 2021; Larsen et al., 2021). This large-scale outbreak resulted in an estimated 4,000 mink-associated human cases and prompted the Danish government to cull all 17 million farmed mink in the country, and several countries imposed total travel bans on the affected regions (Ministry of Environment and Food of Denmark, 2020). Of particular concern was the increased acquisition of spike mutations in mink-associated SARS-CoV-2 viruses, as demonstrated by the Cluster 5 variant identified in September 2020, which had several additional changes in the spike glycoprotein, including Δ69-70 in the N-terminal domain (NTD), and I692V and M1229I in S2 (Lassaunière et al., 2021). Early data indicated a possible change in antigenicity whereby Cluster 5 variant virus might be less readily neutralized by antibodies in convalescent sera from individuals infected by earlier variants (Hoffmann et al., 2021; Lassaunière et al., 2021).

Ferrets are closely related to mink (both belong to the family Mustelidae) and have been used extensively as models for transmission of influenza virus due to their high susceptibility, comparable tissue tropism, and clinical signs similar to those seen in infected humans (Belser et al., 2018). Consequently, ferrets have also been extensively characterized as models for SARS-CoV-2 transmission experiments and can support infection and transmission (Kim et al., 2020; Peacock et al., 2021a; Richard et al., 2020). During experimental infection of SARS-CoV-2 in ferrets, several groups have independently reported mink-associated spike mutations Y453F or N501T (Everett et al., 2021; Oude Munnink et al., 2020; Richard et al., 2020). Mink and ferret ACE2 are extremely similar, with no amino acid differences that map to the ACE2/SARS-CoV-2 spike interface (Figure S1). Interestingly, both the Y453F and the N501T substitutions have also been associated with increased binding to human ACE2 (Starr et al., 2020). It is possible these mutations may act to nonspecifically increase binding to several groups of mammalian ACE2 proteins. A similar mutation N501Y, which is also associated with increased human ACE2 binding, is often found upon mouse adaptation of SARS-CoV-2 and is present in several human SARS-CoV-2 variants of concern showing signs of higher transmissibility (Naveca et al., 2021; Rambaut et al., 2020b; Tegally et al., 2021). It has been hypothesized for influenza virus that increasing receptor binding avidity can result in nonspecific antibody escape as the viral glycoprotein-host receptor interaction begins to outcompete that of antibody/viral glycoprotein (Hensley et al., 2009).

In this study, we risk assess mink- or ferret-adapted viruses and mutations to determine the threat that viruses adapted to mustelid species could pose to humans, and what impact they could have on global vaccine efforts.

RESULTS

Y435F and N501T substitutions in the spike are detected in viruses transmitted between ferrets

In a previous study, we experimentally infected four donor ferrets and tested the ability of SARS-CoV-2 to transmit to individually co-housed naive animals (Peacock et al., 2021a). The early wild-type (WT) virus isolate, England/2/2020, which contains 614D, transmitted efficiently to two of four ferrets in direct contact with two infected donor animals (donor #1 and #2; Figure 1A). Here, we sequenced the spike RBD of virus extracted from nasal wash obtained at early and late time point from the direct contact ferrets. Of the two transmitted virus isolates, at the consensus level, one had gained N501T in the spike protein while the other had a mixture of Y453F and N501T. Both Y453F and N501T have previously been associated with experimental ferret adaptation of SARS-CoV-2 (Everett et al., 2021; Richard et al., 2020). To investigate the dynamics of ferret adaptation in more detail, virus samples were deep sequenced from various time points across the two successful ferret transmission chains (donor #1 to contact #1 and donor #2 to contact #2; Figure 1A). In donor animal #1, the virus rapidly gained majority N501T, with Y453F as a minor variant. However, by day 5, both mutations were present in equal amounts with no detectable WT spike. In the matched contact animal (contact #1), the transmitted virus population included a mixture of Y453F with a minority of N501T and Y453F continued to predominate between days 4 and 6. In Donor/Contact pair #2, again both mutations were detected, but N501T predominated across both animals at all time points tested. N501T alone predominated in the day 2 nasal washes from the two donor animals that did not transmit to their direct contacts (98% in one, 94% in the other), with remaining reads showing WT spike (Peacock et al., 2021a). In the initial virus inoculum, N501T was detected at levels below 1% of total reads while Y453F was not detected at all (read depth ≈7,000). No other consensus-level mutations arose in any of the donor or contact ferrets anywhere else in the genome.

Interestingly, by investigating all SARS-CoV-2 sequences isolated from mink reported on the Global Initiative on Sharing All Influenza Data (GISAID), we and others noted that N501T, Y453F, as well as F486L have independently arisen multiple times in mink, and in multiple lineages, as illustrated in Figure 1B (Lu et al., 2021; Oude Munnink et al., 2020). These observations further imply that these mutations are strongly associated with mustelid adaptation (Figure 1B).

Of all the mink-adapting substitutions, Y453F has been more frequently associated with spillback from mink into humans, including Cluster 5 in Denmark. To further investigate the effects of the Y453F substitution, we isolated virus from contact #1 from day 6 in Vero cells (“Ferret P2”) and validated that the sequence change was maintained in the titrated virus stock (Figure 2A). The Vero-grown virus stock was, in the majority, Y453F (∼96%) with very minor variants, N501T and WT RBD also present (<5%).

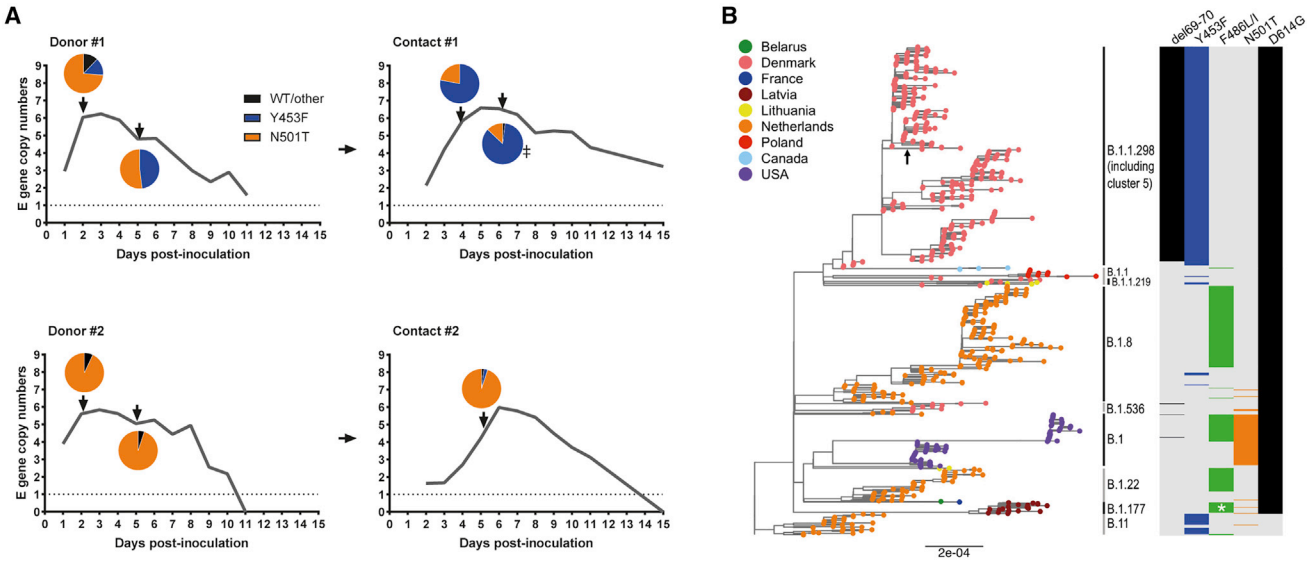

Figure 1. Passage of SARS-CoV-2 in ferrets results in spontaneous emergence of the mink-associated mutations Y453F and N501T

(A) Ferret transmission chains from a previous study were deep sequenced to investigate any changes that occurred during infection and transmission of ferrets. Gray lines indicate previously described RNA shedding patterns seen in each ferret – pie charts indicate RBD mutations seen at each time point (as determined by deep sequencing) indicated by a black arrow. Sample from "Contact #1" marked with double dagger indicates virus that was used for subsequent experiments in Figure 2.

(B) Maximum-likelihood phylogeny of SARS-CoV-2 genomes sampled from American mink (*Neogale vison*, formerly *Neovison vison*), highlighting the spike mutations Δ69-70, Y453F, F486L, or F486I, N501T, and D614G. Tip nodes are shown as points colored by sampling location, according to the color key. Columns to the right show the presence of either the WT amino acid(s) (light gray) or the mutations annotated above (colored bars). Major epidemiological lineages designated with the Pango nomenclature system are labeled. Black arrow indicates the branch that constitutes the Danish mink strain known as Cluster 5. At position 486, mutant viruses possessed 486L (leucine) except for a monophyletic clade formed of 20 sequences sampled in Latvia that possessed 486I (isoleucine) that are marked by a white asterisk.

Outside of spike, the virus contained an additional mutation, S6L in the envelope gene (E), which was present in >70% of reads in the Vero-grown stock.

Virus with Y453F shows enhanced replication and trended toward higher morbidity in ferrets

To investigate whether the Y453F-containing virus showed greater replication in ferrets, we intranasally inoculated four naive ferrets with ferret P2 virus and compared levels of virus shed from the nose with four ferrets previously inoculated with the same infectious titer of parental England/2/2020 virus (Peacock et al., 2021a) (the same donors from Figure 1A). At days 1 to 2, the mean titer of Y453F virus shed in nasal washes was significantly higher than that of the parental virus, as determined by both E gene copy number and median tissue culture infectious dose ($TCID_{50}$) (Figures 2B and 2C). Both groups of ferrets showed comparable patterns of fever during infection, peaking between days 2 and 4, and the Y453F-infected ferrets trended toward more weight loss over the course of the experiment (Figures 2D and 2E). The titer of parental virus shed and fever in parental virus-infected animals approached that in the ferret P2 infected animals by days 3 to 4, likely because the parental virus had gained ferret-adapting mutations, such as Y453F or N501T, by this point (see Figure 1A). Deep sequencing of the virus from the ferrets inoculated with the Y453F-containing ferret P2 virus showed the Y453F substitution was maintained in all four animals throughout the course of infection (Figure 2F). The E gene substitution S6L, however, was rapidly selected against, indicating that this substitution could have been an adaptation to cell culture, selected in Vero cells during isolation and amplification of the virus from nasal wash (Figure 2G). Several further substitutions, all present at very low levels in the inoculum, rapidly grew to fixation in all four Y453F-infected ferrets. These encoded mutations in spike at D614N, in N protein at R68P, and in the NSP2 protein at T632I (Figure 2G). It is unclear whether these substitutions are all *bona fide* ferret adaptations or mutations hitchhiking as part of a selective sweep. Spike D614N may exert a similar effect to the ubiquitous SARS-CoV-2 human adaptation D614G, to nonspecifically enhance ACE2 binding by promoting the spike open conformation (Juraszek et al., 2021). Overall, these data suggest that Y453F adapts the virus to ferret infection, but also further adaptations may arise during ongoing adaptation in mustelid hosts.

Y453F enhances cell entry using the mustelid ACE2 receptor

Next, we tested whether Y453F and the other mustelid-associated spike mutations improved the use of the otherwise suboptimal ferret ACE2 (Conceicao et al., 2020). We created a library of spike expression constructs, generated lentivirus-based pseudoviruses, and assessed the entry of these into cells transiently expressing ACE2 from human, ferret, or rat, or empty vector, as

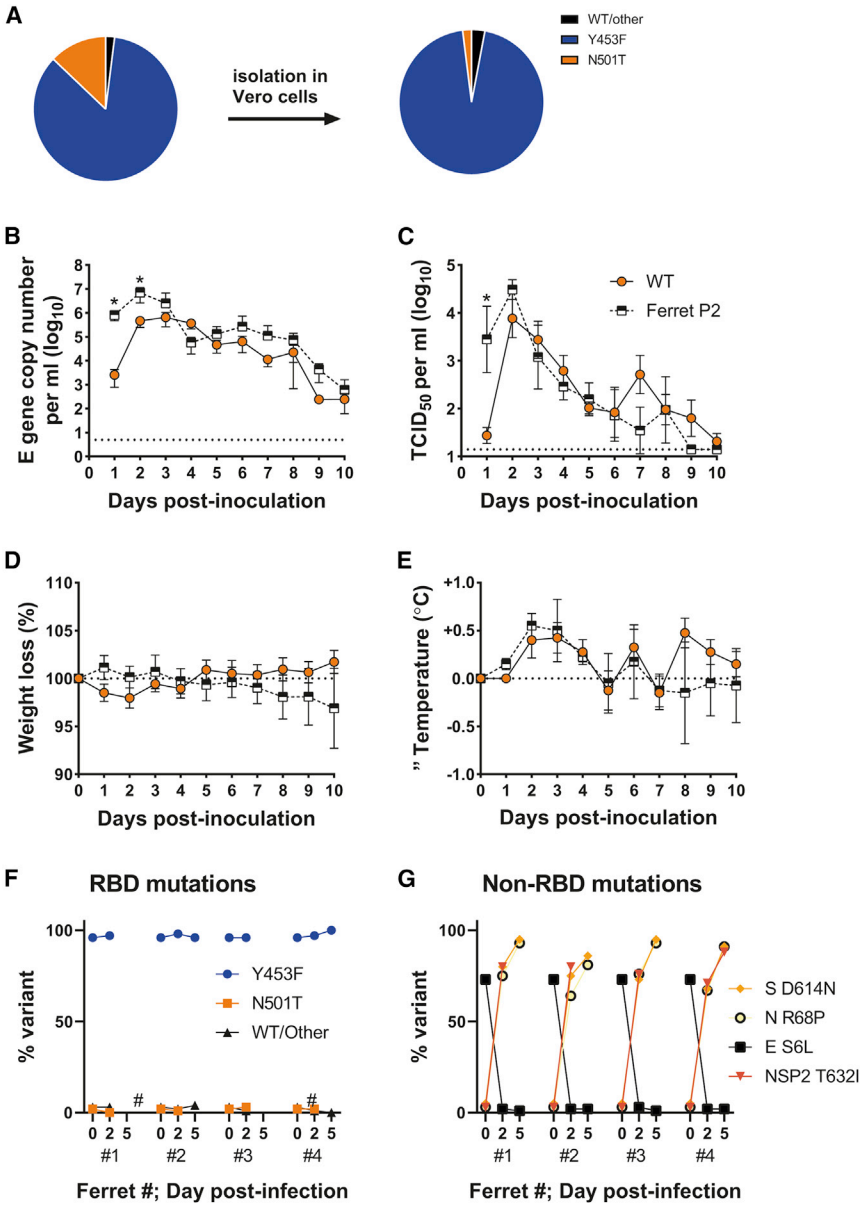

Figure 2. The spike mutation, Y453F, enhances replication and morbidity in ferrets

(A) Deep sequencing of RBD mutations of SARS-CoV-2 from ferret passage 2 swab (see Figure 1A) before and after isolation in Vero cells.

(B–E) RNA (B) and infectious virus (C) shedding dynamics of ferrets directly infected with either WT (orange circles; as previously described in Peacock et al. [2021a]) or Y453F (i.e., ferret passage 2; black and white squares) SARS-CoV-2. n = 4 naive ferrets in each group were infected with 10^5 p.f.u. of either virus. Percentage weight loss (D) and change in body temperature (E) were recorded daily. Data plotted as mean ± s.d. Statistics on (B) and (C) determined by multiple Mann-Whitney tests. *0.05 ≥ *P*.

(F and G) Spike RBD (F) and non-RBD (G) mutations seen in Vero-grown ferret passage 2 virus (time 0) from Figures 2A–2D and dynamics over time in directly infected ferrets. Hash sign marks samples with insufficient coverage to determine sequence proportions.

previously described (Conceicao et al., 2020). We note that ferret ACE2 differs from that of mink by only two amino acid residues that are distal to the spike interaction interface, and therefore can be considered representative for both mustelid species (see Figure S1).

While WT (D614G) spike uses ferret ACE2 poorly for entry (>10-fold less well than human ACE2), the adaptations Y453F, N501T, or F486L, as well as full Cluster 5 spike (Δ69/70, Y453F, D614G, I692V, M1229I), all allowed SARS-CoV-2 spike expressing pseudoviruses to enter into human or ferret, but not rat, ACE2-expressing cells with much greater efficiency (Figures 3A and 3B). A nearby substitution, L452M, which has also appeared in at least one mink farm outbreak (Lu et al., 2021) has no effect, suggesting this is not a specific adaptation to mink (Figure 3A). The effect of Y453F was not dependent on the presence or absence of D614G, as Y453F in a 614D background showed a similar effect (Figure 3C). Consistent results were also seen using a cell-cell fusion assay (Figures S2A and S2B). Examining the structure of the spike RBD/ACE2 interface, each of these mink/ferret adaptations is close to residues that differ between human and mustelid ACE2, as others have previously modeled (Welkers et al., 2020). For example, Spike-Y453F lies close to ACE2-34 (histidine in human ACE2, tyrosine in mustelid), Spike-N501T lies close to ACE2-354, and Spike-F486L lies between ACE2 residues 79, 82, and 24 (Figure 3D).

Viruses containing Y453F mutation are attenuated for replication in primary human airway epithelial cells

To assess the impact of the Y453F mutation on the replication of virus in human airway epithelium, we infected primary human bronchial cells cultured at an air-liquid interface with a mix of the parental and ferret P2 viruses at a low multiplicity of infection (MOI) of around 0.1 (Figure 4A). Samples were taken 24, 48, and 72 h postinfection and analyzed by deep sequencing. The WT virus significantly outcompeted Y453F, with less than ~5% of reads by 48 h postinfection containing Y453F.

Although the Y453F-containing virus is highly similar to that which circulated in mink early in the pandemic, the most prominent zoonotic spillover from mink was the Cluster 5 virus, which further contained D614G and Δ69-70. D614G and Δ69-70 are thought to potentially enhance virus infectivity in some backgrounds (Meng et al., 2021). Therefore, we performed a similar competition experiment between a mixed inoculum of 40%

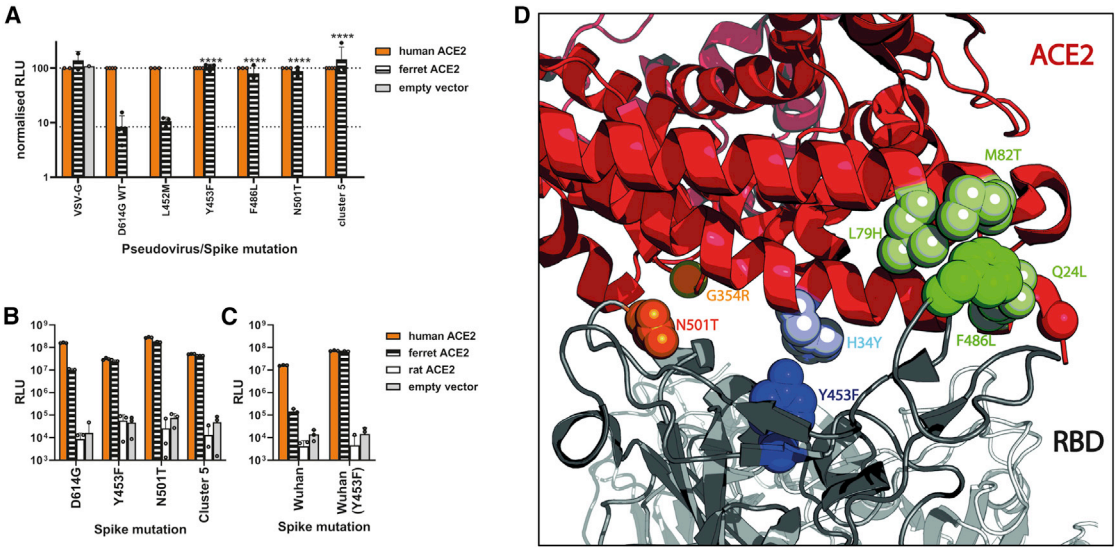

Figure 3. Mink- and ferret-associated spike mutations allow more efficient entry into cells expressing the ferret ACE2 receptor

(A) Pseudovirus entry in human or ferret ACE2-expressing cells. Mutant SARS-CoV-2 spike-containing pseudovirus entry into HEK 293Ts expressing human or ferret ACE2 or empty vector. Entry normalized to signals from human ACE2 expressing cells. Each data point indicates mean value taken from a completely independent repeat ($n \geq 3$). Data plotted as mean ± s.d. Statistics were determined by comparing log-transformed values of ferret ACE2 entry using a one-way ANOVA with multiple comparisons against the WT. *$0.05 \geq p > 0.01$; **$0.01 \geq p > 0.001$; ***$0.001 \geq p > 0.0001$; ****$p \leq 0.0001$.

(B and C) Entry of SARS-CoV-2 spike mutant-expressing lentiviral pseudotypes into BHK-21 cells expressing different mammalian ACE2 proteins. Pseudovirus shown contain either D614G (B) or D614 (C). Representative repeat shown from $n \geq 3$ repeats. Data plotted as mean ± s.d.

(D) Structure of ACE2/Spike RBD interface showing key mink-adaptation residues and nearby residues that differ in mustelid and human ACE2. Figure made using PyMOL (Schrödinger) and PDB: 7A94(Benton et al., 2020).

Cluster 5 isolate and 60% early B.1 lineage, D614G containing virus ("WT"; IC19). Again, we observed that the Y453F-containing Cluster 5 was outcompeted, constituting only ~10% of reads by 24 h postinfection (Figure 4B).

Finally, to further confirm that the attenuation in human cells of the Y453F-containing viruses, particularly the ferret-adapted strain, was not due to other changes in the genome (such as E S6L described above), we generated by reverse genetics (RG) two isogenic viruses on a Wuhan-hu-1 backbone, both carrying the D614G mutation in spike, WT (D614G), while the other additionally contained Y453F (D614G + Y453F). As with the ferret-adapted P2 virus and Cluster 5 isolate we saw that the Y453F + D614G RG virus produced less infectious virus upon replication in the primary human airway cells as compared with the otherwise isogenic WT (D614G) virus, significantly so at 24 h postinfection (Figure 4C).

Mink adaptation has a minimal effect on SARS-CoV-2 antigenicity

To investigate whether a mustelid-adapted SARS-CoV-2 crossing back into the human population would have a large impact on re-infections or vaccine-breakthrough, we next tested whether the mutation at Y453F facilitated escape from antibody neutralization. Surprisingly, Y453F-containing "Ferret P2" virus was significantly *more easily* neutralized by convalescent first-wave antisera than WT requiring only 0.6 as much antisera for a 50% neutralization titer (Figure 5A). We further investigated the relative antigenicity of Y453F, this time using the above-described RG viruses and antisera from health care workers who had received two doses the of Pfizer-BioNtech-BNT162b2 vaccine. Again, we saw the Y453F-containing virus was more readily neutralized by 7 of the 10 vaccinee sera, although the difference was not significant (Figure 5B).

We next performed pseudovirus neutralization assays with the previously described first-wave convalescent antisera against pseudoviruses expressing the common mustelid adaptations or with full Cluster 5 spike. The B.1.351 (Beta) spike showed a significant, ~5-fold drop in mean 50% neutralization titer (NT_{50}) (Figure 5C), consistent with this virus being more difficult to neutralize with first-wave antisera (Garcia-Beltran et al., 2021). None of the tested mink/ferret adaptations had any significant impact on antigenicity.

Many circulating variants of concern show a greater ability to enter via mustelid ACE2

Following worldwide circulation of SARS-CoV-2, a number of "variant of concern" and "variant of interest" lineages have arisen associated with properties, such as increased transmissibility, higher pathogenicity, and antigenic escape (Peacock et al., 2021b). These generally locally, or globally, outcompeted other lineages to become predominant, including the Alpha variant (B.1.1.7), first associated with infections the United Kingdom (Rambaut et al., 2020b). A number of these variants have RBD mutations such as L452R, E484K, and/or N501Y, which are thought to promote human ACE2 binding (Starr et al., 2020).

To investigate whether these variants may be more able to infect mink or ferrets than the progenitor lineage B or B.1 viruses through better use of mustelid ACE2, we again used

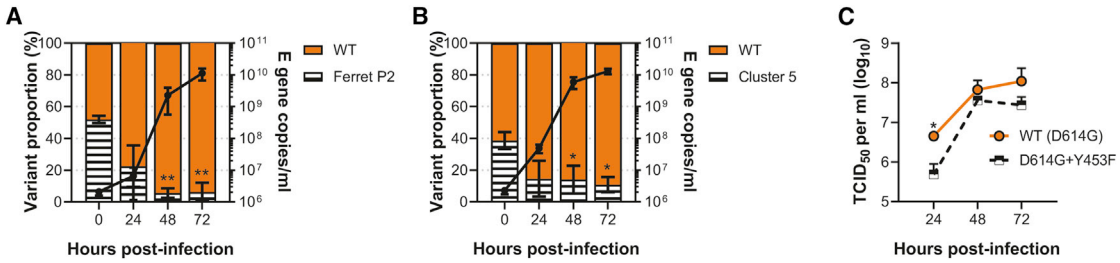

Figure 4. The common mink and ferret adaptation, Y453F, attenuates virus replication in primary human airway cells

(A–C) Human primary airway epithelial cells cultured at air-liquid interface were infected at an MOI of approximately 0.1 with (A) a mixture of parental and ferret-adapted England/2 virus, (B) a mixture of mink-adapted "Cluster 5" virus and a D614G control, or (C) either isogenic WT (D614G) or D614G + Y453F -containing reverse genetics-derived virus isolates. Virus titers were measured by $TCID_{50}$ (C) E gene qPCR (A, B). Statistics for competition assays were determined by one-way ANOVA with multiple comparisons against time 0. Statistics for the head-to-head growth curve (C) were determined by multiple unpaired t tests on log-transformed data. All infections were performed on triplicate wells from matched donors (n = 3). Data plotted as mean ± s.d. *0.05 ≥ p > 0.01; **p ≤ 0.01.

pseudoviruses expressing these variant spike proteins and normalized entry to human ACE2 (Figure 6). We found that nearly all variants of concern tested could better use mink ACE2 than WT (D614G only) pseudovirus. B.1.1.7/E484K, Iota/B.1.526 + E484K (first associated with infections in New York), Eta/B.1.525 (a variant with associations with West Africa), and L452R (in multiple variants of concern, including Epsilon/B.1.427/B.1.429, first associated with infections in California, and Delta/B.1.617.2, which is currently replacing all other SARS-CoV-2 lineages globally) all allowed pseudovirus to use ferret ACE2 for cell entry to almost the same degree as human ACE2. Alpha/B.1.1.7 and Beta/B.1.351 spikes showed a much more modest boost, while Gamma/P.1 (first found in Japan in travelers from Brazil) showed no improved usage of ferret ACE2. It appears L452R, E484K, and N501Y may promote use of ferret ACE2, while K417N/T may result in a greater reduction in ferret ACE2 usage relative to human ACE2. Overall, these data suggest multiple circulating variants of concern may be able to infect mustelid hosts with only minimal, or indeed without, further adaptation.

DISCUSSION

In this study, we have performed a full risk assessment of mustelid hosts, such as mink and ferrets, as reservoirs for the emergence of antigenic variants or new variants of concern. We have shown earlier strains of SARS-CoV-2 are poorly adapted to mustelid ACE2 and therefore quickly gain adaptations, such as Y453F, N501T, or F486L to use mustelid ACE2. However, Y453F in particular, negatively impacts replication kinetics of SARS-CoV-2 in human cells, potentially explaining why the Danish mink-origin outbreaks did not propagate further following the culling of the mink. Furthermore, in line with other studies (Garcia-Beltran et al., 2021; Hoffmann et al., 2021; Lassaunière et al., 2021), we found none of these mutations had a large antigenic impact, so vaccination is likely to remain effective against

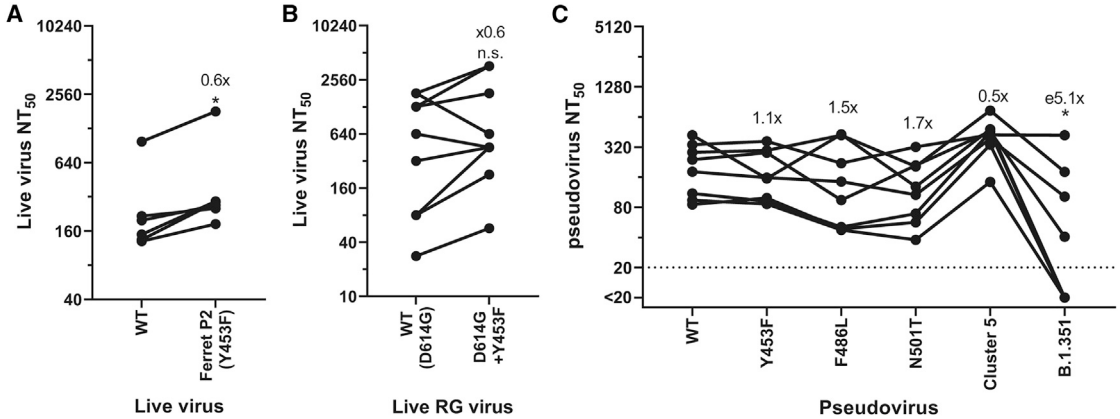

Figure 5. Mink- and ferret-associated mutations have a minimal impact on SARS-CoV-2 antigenicity

(A and B) Live virus neutralization comparing WT or Y453F-containg ferret passage 2 (A) or the isogenic reverse genetics-derived WT (D614G) and D614G + Y453F-containing SARS-CoV-2 isolates (B) using N = 6 human convalescent antisera from the first UK wave (~April-June 2020); (A) or n = 10 double-dose BNT162b2 (Pfizer-BioNTech mRNA vaccine) human antisera (B). Fold differences annotated on graph indicate differences in geometric means of NT_{50}. Statistics were determined by two-tailed Wilcoxon test with matched pairs. *0.05 ≥ *P*.

(C) Pseudovirus neutralization of different mink adaptations containing mutants using N = 8 human convalescent antisera from the first UK wave (~April-June 2020). Fold differences annotated on graph indicate differences in geometric means of NT_{50}. Statistics determined by matched pair Friedman nonparametric test with multiple comparisons against WT. *0.05 ≥ *P*.

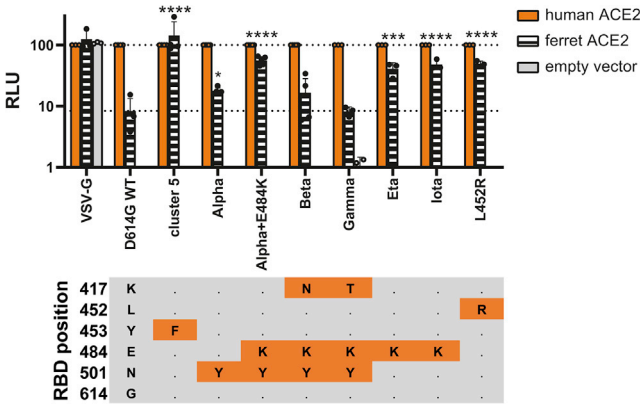

Figure 6. Several variants of concern show enhanced entry into ferret ACE2 expressing cells

Mutant SARS-CoV-2 spike-containing pseudovirus entry into HEK 293Ts expressing human or ferret ACE2, or empty vector. Entry normalized to signals from human ACE2 expressing cells. Each data point indicates data from a completely independent repeat ($n \geq 3$). Data plotted as mean ± s.d. Statistics were determined by comparing log-transformed values of ferret ACE2 entry using a one-way ANOVA with multiple comparisons against the WT. *$0.05 \geq p > 0.01$; **$0.01 \geq p > 0.001$; ***$0.001 \geq p > 0.0001$; ****$p \leq 0.0001$. RBD mutational profile of the different spike proteins is shown below. Cells in orange indicate changes from WT/D614G. Alpha also known as B.1.1.7; Beta also known as B.1.351; Gamma also known as P.1; Eta also known as B.1.525; Iota also known as B.1.526 + E484K.

mustelid-adapted strains. Finally, we have shown that several variant of concern (VOC) strains, or VOC-associated mutations, partially adapt SARS-CoV-2 spike to mustelid ACE2. Therefore, it is likely VOC lineages will continue to infect mink farms and risk spilling back over into humans.

Except for the Danish mink-adapted SARS-CoV-2 spillback, Y453F is found rarely in humans with very few isolates reported in GISAID and only a single report of the mutation arising in immunocompromised patients – this is despite Y453F having been shown in several studies to enhance human ACE2 binding, in a similar manner to the VOC-associated mutations N501Y or L452R (Bayarri-Olmos et al., 2021; Motozono et al., 2021; Starr et al., 2020). This would suggest that unlike the VOC-associated mutations, such as N501Y, Y453F attenuates viral fitness in human cells, we speculate this could be due to the previously described destabilization of the spike caused by Y453F outweighing any potential increase in human ACE2 binding (Motozono et al., 2021). We have shown that, even in the presence of the putative stabilizing NTD deletion, Δ69-70 (Meng et al., 2021), virus harboring the Y453F substitution was outcompeted by a closely related virus in human cells.

Here, we have demonstrated many VOCs, particularly Alpha/B.1.1.7 as well as those containing L452R (such as Delta/B.1.617.2), could have a fundamental fitness advantage in mink by increasing interaction with mustelid ACE2, compared with previous nonvariant strains. At present (August 2021), the vast majority of mink-origin SARS-CoV-2 sequences on GISAID are from the year 2020, even though there are a number of ongoing mink outbreaks reported in Europe (Author Anonymous 2021a; 2021b), suggesting a significant reporting lag. None of the four World Health Organization-designated VOCs have yet been associated with mink farm outbreaks. It remains to be seen whether these VOCs would replicate in minks/ferrets without any further adaptation, but we have shown that the most common mustelid adaptations would be unlikely to have a large effect on VOC antigenicity. It will be key in the coming years to continue to closely survey farmed mink and to sequence and share any SARS-CoV-2 genomes from these animals in a timely manner, as SARS-CoV-2 could still adapt in unexpected ways in mink (Goldhill and Barclay, 2021).

This work also suggests that, particularly when investigating spike RBD mutants, ferrets (or indeed mink) are poor models for humans, as mustelid ACE2 is poorly used by nonadapted SARS-CoV-2 spike. Thus, it is not a given that adaptation to human ACE2 will also result in increased infectiousness, transmissibility, or pathogenicity in the ferret model. However, ferrets remain a useful model for investigating non-RBD phenotypes, although care should be taken to use previously ferret-adapted viruses to prevent rapid adaptation.

Limitations of the study

Although this work has taken a multidisciplinary approach with experiments often performed in parallel over different sites a number of limitations remain, one of which is the overreliance on ferrets and ferret ACE2 as a substitution for mink/mink ACE2. Another limitation is that only Y453F-containing viruses were followed up for in depth virological study, therefore this work cannot make strong conclusions about the zoonotic potential of the other mink adaptations that often appear, particularly N501T, which has subsequently appeared on several human SARS-CoV-2 variant lineages. Finally, this work has used entry of pseudovirus in ferret ACE2-overexpressing cells as a proxy for ACE2 usage rather than quantitively measuring the direct interaction between Spike RBD and ACE2 binding.

STAR★METHODS

Detailed methods are provided in the online version of this paper and include the following:

- KEY RESOURCES TABLE
- RESOURCE AVAILABILITY
  - Lead contact
  - Materials availability
  - Data and code availability
- EXPERIMENTAL MODEL AND SUBJECT DETAILS
  - Ferrets (Mustela putorius furo)
  - Cells
- METHOD DETAILS
  - Biosafety and ethics statement
  - Viruses, reverse genetics, and growth kinetics
  - E gene RT-qPCR
  - Live virus neutralisation
  - Plasmids and cloning
  - Pseudovirus assays
  - Cell-cell fusion assay
  - Ferret infection study

- RNA extraction and sequencing
- Phylogenetic analysis

- QUANTIFICATION AND STATISTICAL ANALYSIS

SUPPLEMENTAL INFORMATION

Supplemental information can be found online at https://doi.org/10.1016/j.celrep.2022.110344.

ACKNOWLEDGMENTS

The SARS-CoV-2 virus isolate, England/2, was provided by Public Health England, and we thank M. Zambon, R. Gopal, and M. Patel for their help. The authors also thank Kevin Bewley of Public Health England for help obtaining the Cluster 5 isolate, SARS-CoV-2/hu/DK/CL-5/1, and Michelle Willicombe, Maria Prendecki, and Candice Clarke for their help obtaining the Pfizer double-dose antisera. We also thank E. J. Louis, University of Leicester for generously providing the TAR in yeast system. The authors thank all researchers who have shared genome data openly via the Global Initiative on Sharing All Influenza Data (GISAID).

This work was supported by the G2P-UK National Virology Consortium funded by the MRC (MR/W005611/1). Additional funding to D.B., A.M., N.T., and G.G. was by The Pirbright Institute's BBSRC institute strategic program grant (BBS/E/I/00007038). SARS-CoV-2 research for J.A.H., R.P.R., H.G., I.D.-B., X.D., and N.P.R. is supported by the U.S. Food and Drug Administration (FDA) Medical Countermeasures Initiative contract (5F40120C00085). The work at the CVR was also supported by the MRC grants (MC_UU12014/2) and the Wellcome Trust (206369/Z/17/Z).

The article reflects the views of the authors and does not represent the views or policies of the FDA.

AUTHOR CONTRIBUTIONS

J.Z., T.P.P., J.B., D.H.G., D.B., and W.S.B. conceived and planned the experiments. J.Z., T.P.P., J.C.B., D.H.G., A.M.E.E., R.P.-R., V.M.C., G.D.L., W.F., W.T.H., R.K., L.B., R.F., R.L., N.T., G.G., H.G., I.D.-B., X.D., N.P.R., F.S., M.C.G., and P.F.M. performed the experiments and analyzed the data. A.H.P., M.P., J.A.H., D.B., and W.S.B. provided supervision. T.P.P. and W.S.B. wrote the manuscript with input from all other authors.

DECLARATION OF INTERESTS

The authors declare no competing interests.

Received: September 1, 2021
Revised: November 11, 2021
Accepted: January 14, 2022
Published: February 8, 2022

REFERENCES

Author Anonymous. (2021a). Poland Orders Cull at Fur Farm with Country's First Mink Coronavirus Case (Notes from Poland). https://notesfrompoland.com/2021/02/01/poland-orders-cull-at-fur-farm-with-countrys-first-mink-coronavirus-case/.

Author Anonymous. (2021b). Renewed calls for closure of Galicia mink farms after four more Covid outbreaks. In Spanish News Today. https://spanishnewstoday.com/renewed-calls-for-closure-of-galicia-mink-farms-after-four-more-covid-outbreaks_1612810-a.html.

Bayarri-Olmos, R., Rosbjerg, A., Johnsen, L.B., Helgstrand, C., Bak-Thomsen, T., Garred, P., and Skjoedt, M.-O. (2021). The SARS-CoV-2 Y453F mink variant displays a pronounced increase in ACE-2 affinity but does not challenge antibody neutralization. J. Biol. Chem. *296*, 100536.

Belser, J.A., Barclay, W., Barr, I., Fouchier, R.A.M., Matsuyama, R., Nishiura, H., Peiris, M., Russell, C.J., Subbarao, K., Zhu, H., et al. (2018). Ferrets as models for influenza virus transmission studies and pandemic risk assessments. Emerg. Infect. Dis. *24*, 965–971.

Benton, D.J., Wrobel, A.G., Xu, P., Roustan, C., Martin, S.R., Rosenthal, P.B., Skehel, J.J., and Gamblin, S.J. (2020). Receptor binding and priming of the spike protein of SARS-CoV-2 for membrane fusion. Nature *588*, 327–330.

Brown, J.C., Goldhill, D.H., Zhou, J., Peacock, T.P., Frise, R., Goonawardane, N., Baillon, L., Kugathasan, R., Pinto, A.L., McKay, P.F., et al. (2021). Increased transmission of SARS-CoV-2 lineage B.1.1.7 (VOC 2020212/01) is not accounted for by a replicative advantage in primary airway cells or antibody escape. bioRxiv.

Conceicao, C., Thakur, N., Human, S., Kelly, J.T., Logan, L., Bialy, D., Bhat, S., Stevenson-Leggett, P., Zagrajek, A.K., Hollinghurst, P., et al. (2020). The SARS-CoV-2 Spike protein has a broad tropism for mammalian ACE2 proteins. PLoS Biol. *18*, e3001016.

Corman, V.M., Landt, O., Kaiser, M., Molenkamp, R., Meijer, A., Chu, D.K., Bleicker, T., Brünink, S., Schneider, J., Schmidt, M.L., et al. (2020). Detection of 2019 novel coronavirus (2019-nCoV) by real-time RT-PCR. Euro Surveill. *25*, 2000045.

Davidson, A.D., Williamson, M.K., Lewis, S., Shoemark, D., Carroll, M.W., Heesom, K.J., Zambon, M., Ellis, J., Lewis, P.A., Hiscox, J.A., et al. (2020). Characterisation of the transcriptome and proteome of SARS-CoV-2 reveals a cell passage induced in-frame deletion of the furin-like cleavage site from the spike glycoprotein. Genome Med. *12*, 68.

Dong, X., Munoz-Basagoiti, J., Rickett, N.Y., Pollakis, G., Paxton, W.A., Günther, S., Kerber, R., Ng, L.F.P., Elmore, M.J., Magassouba, N.f., et al. (2020). Variation around the dominant viral genome sequence contributes to viral load and outcome in patients with Ebola virus disease. Genome Biol. *21*, 238.

Everett, H.E., Lean, F.Z.X., Byrne, A.M.P., van Diemen, P.M., Rhodes, S., James, J., Mollett, B., Coward, V.J., Skinner, P., Warren, C.J., et al. (2021). Intranasal infection of ferrets with SARS-CoV-2 as a model for asymptomatic human infection. Viruses *13*, 113.

Flower, B., Brown, J.C., Simmons, B., Moshe, M., Frise, R., Penn, R., Kugathasan, R., Petersen, C., Daunt, A., Ashby, D., et al. (2020). Clinical and laboratory evaluation of SARS-CoV-2 lateral flow assays for use in a national COVID-19 seroprevalence survey. Thorax *75*, 1082–1088.

Gaida, A., Becker, M.M., Schmid, C.D., Bühlmann, T., Louis, E.J., and Beck, H.-P. (2011). Cloning of the repertoire of individual plasmodium falciparum var genes using transformation associated recombination (TAR). PLoS One *6*, e17782.

Garcia-Beltran, W.F., Lam, E.C., St Denis, K., Nitido, A.D., Garcia, Z.H., Hauser, B.M., Feldman, J., Pavlovic, M.N., Gregory, D.J., Poznansky, M.C., et al. (2021). Multiple SARS-CoV-2 variants escape neutralization by vaccine-induced humoral immunity. Cell *184*, 2372–2383.e79.

Goldhill, D.H., and Barclay, W.S. (2021). 2020 hindsight - should evolutionary virologists have expected the unexpected during a pandemic? Evolution *75*, 2311–2316.

Gu, H., Chen, Q., Yang, G., He, L., Fan, H., Deng, Y.-Q., Wang, Y., Teng, Y., Zhao, Z., Cui, Y., et al. (2020). Adaptation of SARS-CoV-2 in BALB/c mice for testing vaccine efficacy. Science *369*, 1603–1607.

Hammer, A.S., Quaade, M.L., Rasmussen, T.B., Fonager, J., Rasmussen, M., Mundbjerg, K., Lohse, L., Strandbygaard, B., Jørgensen, C.S., Alfaro-Núñez, A., et al. (2021). SARS-CoV-2 transmission between mink (Neovison vison) and humans, Denmark. Emerg. Infect. Dis. *27*, 547–551.

Hensley, S.E., Das, S.R., Bailey, A.L., Schmidt, L.M., Hickman, H.D., Jayaraman, A., Viswanathan, K., Raman, R., Sasisekharan, R., Bennink, J.R., et al. (2009). Hemagglutinin receptor binding avidity drives influenza A virus antigenic drift. Science *326*, 734–736.

Hoffmann, M., Kleine-Weber, H., and Pöhlmann, S. (2020a). A multibasic cleavage site in the spike protein of SARS-CoV-2 is essential for infection of human lung cells. Mol. Cell *78*, 779–784.e5.

Hoffmann, M., Kleine-Weber, H., Schroeder, S., Kruger, N., Herrler, T., Erichsen, S., Schiergens, T.S., Herrler, G., Wu, N.H., Nitsche, A., et al. (2020b). SARS-CoV-2 cell entry depends on ACE2 and TMPRSS2 and is blocked by a clinically proven protease inhibitor. Cell *181*, 271–280.e8.

Hoffmann, M., Zhang, L., Krüger, N., Graichen, L., Kleine-Weber, H., Hofmann-Winkler, H., Kempf, A., Nessler, S., Riggert, J., Winkler, M.S., et al. (2021). SARS-CoV-2 mutations acquired in mink reduce antibody-mediated neutralization. Cell Rep. *35*, 109017.

Ishikawa, H., Meng, F., Kondo, N., Iwamoto, A., and Matsuda, Z. (2012). Generation of a dual-functional split-reporter protein for monitoring membrane fusion using self-associating split GFP. Protein Eng. Des. Sel. *25*, 813–820.

Juraszek, J., Rutten, L., Blokland, S., Bouchier, P., Voorzaat, R., Ritschel, T., Bakkers, M.J.G., Renault, L.L.R., and Langedijk, J.P.M. (2021). Stabilizing the closed SARS-CoV-2 spike trimer. Nat. Commun. *12*, 244.

Katoh, K., and Standley, D.M. (2013). MAFFT multiple sequence alignment software version 7: improvements in performance and usability. Mol. Biol. Evol. *30*, 772–780.

Kim, Y.I., Kim, S.G., Kim, S.M., Kim, E.H., Park, S.J., Yu, K.M., Chang, J.H., Kim, E.J., Lee, S., Casel, M.A.B., et al. (2020). Infection and rapid transmission of SARS-CoV-2 in ferrets. Cell Host Microbe *27*, 704–709.e2.

Larsen, H.D., Fonager, J., Lomholt, F.K., Dalby, T., Benedetti, G., Kristensen, B., Urth, T.R., Rasmussen, M., Lassaunière, R., Rasmussen, T.B., et al. (2021). Preliminary report of an outbreak of SARS-CoV-2 in mink and mink farmers associated with community spread, Denmark, June to November 2020. Euro Surveill. *26*, 2100009.

Lassaunière, R., Fonager, J., Rasmussen, M., Frische, A., Polacek, C., Rasmussen, T.B., Lohse, L., Belsham, G.J., Underwood, A., Winckelmann, A.A., et al. (2021). In vitro characterization of fitness and convalescent antibody neutralization of SARS-CoV-2 cluster 5 variant emerging in mink at Danish farms. Front. Microbiol. *12*, 698944.

Lu, L., Sikkema, R.S., Velkers, F.C., Nieuwenhuijse, D.F., Fischer, E.A.J., Meijer, P.A., Bouwmeester-Vincken, N., Rietveld, A., Wegdam-Blans, M.C.A., Tolsma, P., et al. (2021). Adaptation, spread and transmission of SARS-CoV-2 in farmed minks and related humans in The Netherlands. bioRxiv.

McKay, P.F., Hu, K., Blakney, A.K., Samnuan, K., Brown, J.C., Penn, R., Zhou, J., Bouton, C.R., Rogers, P., Polra, K., et al. (2020). Self-amplifying RNA SARS-CoV-2 lipid nanoparticle vaccine candidate induces high neutralizing antibody titers in mice. Nat. Commun. *11*, 3523.

Meng, B., Kemp, S.A., Papa, G., Datir, R., Ferreira, I.A.T.M., Marelli, S., Harvey, W.T., Lytras, S., Mohamed, A., Gallo, G., et al. (2021). Recurrent emergence of SARS-CoV-2 spike deletion H69/V70 and its role in the Alpha variant B.1.1.7. Cell Rep. *35*, 109292.

Ministry of Environment and Food of Denmark. (2020). COVID-19: All Mink in Denmark Must Be Culled.

Moshe, M., Daunt, A., Flower, B., Simmons, B., Brown, J.C., Frise, R., Penn, R., Kugathasan, R., Petersen, C., Stockmann, H., et al. (2021). SARS-CoV-2 lateral flow assays for possible use in national covid-19 seroprevalence surveys (React 2): diagnostic accuracy study. BMJ *372*, n423.

Motozono, C., Toyoda, M., Zahradnik, J., Saito, A., Nasser, H., Tan, T.S., Ngare, I., Kimura, I., Uriu, K., Kosugi, Y., et al. (2021). SARS-CoV-2 spike L452R variant evades cellular immunity and increases infectivity. Cell Host Microbe *29*, 1124–1136.e11.

Naveca, F., da Costa, C., Nascimento, V., Souza, V., Corado, A., Nascimento, F., Costa, A., Duarte, D., Silva, G., Mejía, M., et al. (2021). SARS-CoV-2 Reinfection by the New Variant of Concern (VOC) P.1 in Amazonas, Brazil (virological.Org). https://virological.org/t/sars-cov-2-reinfection-by-the-new-variant-of-concern-voc-p-1-in-amazonas-brazil/596.

OIE (2021). Events in Animals. https://www.oie.int/en/scientific-expertise/specific-information-and-recommendations/questions-and-answers-on-2019novel-coronavirus/events-in-animals/.

Oude Munnink, B.B., Sikkema, R.S., Nieuwenhuijse, D.F., Molenaar, R.J., Munger, E., Molenkamp, R., van der Spek, A., Tolsma, P., Rietveld, A., Brouwer, M., et al. (2020). Transmission of SARS-CoV-2 on mink farms between humans and mink and back to humans. Science *371*, 172–177.

O'Toole, Á., Scher, E., Underwood, A., Jackson, B., Hill, V., McCrone, J.T., Colquhoun, R., Ruis, C., Abu-Dahab, K., Taylor, B., et al. (2021). Assignment of epidemiological lineages in an emerging pandemic using the pangolin tool. Virus Evol. *7*, veab064.

Peacock, T.P., Goldhill, D.H., Zhou, J., Baillon, L., Frise, R., Swann, O.C., Kugathasan, R., Penn, R., Brown, J.C., Sanchez-David, R.Y., et al. (2021a). The furin cleavage site in the SARS-CoV-2 spike protein is required for transmission in ferrets. Nat. Microbiol. *6*, 899–909.

Peacock, T.P., Penrice-Randal, R., Hiscox, J.A., and Barclay, W.S. (2021b). SARS-CoV-2 one year on: evidence for ongoing viral adaptation. J. Gen. Virol. *102*, 001584.

Prendecki, M., Clarke, C., Edwards, H., McIntyre, S., Mortimer, P., Gleeson, S., Martin, P., Thomson, T., Randell, P., Shah, A., et al. (2021). Humoral and T-cell responses to SARS-CoV-2 vaccination in patients receiving immunosuppression. Ann. Rheum. Dis. *80*, 1322–1329.

Rabalski, L., Kosinski, M., Smura, T., Aaltonen, K., Kant, R., Sironen, T., Szewczyk, B., and Grzybek, M. (2021). Severe acute respiratory syndrome coronavirus 2 in farmed mink (Neovison vison), Poland. Emerg. Infect. Dis. *27*, 2333–2339.

Rambaut, A., Holmes, E.C., O'Toole, Á., Hill, V., McCrone, J.T., Ruis, C., du Plessis, L., and Pybus, O.G. (2020a). A dynamic nomenclature proposal for SARS-CoV-2 lineages to assist genomic epidemiology. Nat. Microbiol. *5*, 1403–1407.

Rambaut, A., Loman, N., Pybus, O., Barclay, W., Barrett, J., Carabelli, A., Connor, T., Peacock, T., Robertson, D.L., Volz, E., et al. (2020b). Preliminary Genomic Characterisation of an Emergent SARS-CoV-2 Lineage in the UK Defined by a Novel Set of Spike Mutations (virological.Org). https://virological.org/t/preliminary-genomic-characterisation-of-an-emergent-sars-cov-2-lineage-in-the-uk-defined-by-a-novel-set-of-spike-mutations/563/2.

Rathnasinghe, R., Jangra, S., Cupic, A., Martínez-Romero, C., Mulder, L.C.F., Kehrer, T., Yildiz, S., Choi, A., Mena, I., De Vrieze, J., et al. (2021). The N501Y mutation in SARS-CoV-2 spike leads to morbidity in obese and aged mice and is neutralized by convalescent and post-vaccination human sera. medRxiv.

Rebendenne, A., Valadão, A.L.C., Tauziet, M., Maarifi, G., Bonaventure, B., McKellar, J., Planès, R., Nisole, S., Arnaud-Arnould, M., Moncorgé, O., et al. (2021). SARS-CoV-2 triggers an MDA-5-dependent interferon response which is unable to control replication in lung epithelial cells. J. Virol. *95*, e02415–20.

Richard, M., Kok, A., de Meulder, D., Bestebroer, T.M., Lamers, M.M., Okba, N.M.A., Fentener van Vlissingen, M., Rockx, B., Haagmans, B.L., Koopmans, M.P.G., et al. (2020). SARS-CoV-2 is transmitted via contact and via the air between ferrets. Nat. Commun. *11*, 3496.

Rihn, S.J., Merits, A., Bakshi, S., Turnbull, M.L., Wickenhagen, A., Alexander, A.J.T., Baillie, C., Brennan, B., Brown, F., Brunker, K., et al. (2021). A plasmid DNA-launched SARS-CoV-2 reverse genetics system and coronavirus toolkit for COVID-19 research. PLoS Biol. *19*, e3001091.

da Silva Filipe, A., Shepherd, J.G., Williams, T., Hughes, J., Aranday-Cortes, E., Asamaphan, P., Ashraf, S., Balcazar, C., Brunker, K., Campbell, A., et al. (2021). Genomic epidemiology reveals multiple introductions of SARS-CoV-2 from mainland Europe into Scotland. Nat. Microbiol. *6*, 112–122.

Stamatakis, A. (2014). RAxML version 8: a tool for phylogenetic analysis and post-analysis of large phylogenies. Bioinformatics *30*, 1312–1313.

Starr, T.N., Greaney, A.J., Hilton, S.K., Ellis, D., Crawford, K.H.D., Dingens, A.S., Navarro, M.J., Bowen, J.E., Tortorici, M.A., Walls, A.C., et al. (2020). Deep mutational scanning of SARS-CoV-2 receptor binding domain reveals constraints on folding and ACE2 binding. Cell *182*, 1295–1310.e20.

Tegally, H., Wilkinson, E., Giovanetti, M., Iranzadeh, A., Fonseca, V., Giandhari, J., Doolabh, D., Pillay, S., San, E.J., Msomi, N., et al. (2021). Detection of a SARS-CoV-2 variant of concern in South Africa. Nature *592*, 438–443.

Thakur, N., Conceicao, C., Isaacs, A., Human, S., Modhiran, N., McLean, R.K., Pedrera, M., Tan, T.K., Rijal, P., Townsend, A., et al. (2021). Micro-fusion inhibition tests: quantifying antibody neutralization of virus-mediated cell–cell fusion. J. Gen. Virol. *102*, jgv001506.

Thi Nhu Thao, T., Labroussaa, F., Ebert, N., V'kovski, P., Stalder, H., Portmann, J., Kelly, J., Steiner, S., Holwerda, M., Kratzel, A., et al. (2020). Rapid reconstruction of SARS-CoV-2 using a synthetic genomics platform. Nature *582*, 561–565.

Welkers, M.R.A., Han, A.X., Reusken, C.B.E.M., and Eggink, D. (2020). Possible host-adaptation of SARS-CoV-2 due to improved ACE2 receptor binding in mink. Virus Evol. *7*, veaa094.

Wu, F., Zhao, S., Yu, B., Chen, Y.M., Wang, W., Song, Z.G., Hu, Y., Tao, Z.W., Tian, J.H., Pei, Y.Y., et al. (2020). A new coronavirus associated with human respiratory disease in China. Nature *579*, 265–269.

Yan, R., Zhang, Y., Li, Y., Xia, L., Guo, Y., and Zhou, Q. (2020). Structural basis for the recognition of SARS-CoV-2 by full-length human ACE2. Science *367*, 1444–1448.

Yu, G., Smith, D.K., Zhu, H., Guan, Y., and Lam, T.T.-Y. (2017). ggtree: an r package for visualization and annotation of phylogenetic trees with their covariates and other associated data. Methods Ecol. Evol. *8*, 28–36.

Zhao, X., Chen, D., Szabla, R., Zheng, M., Li, G., Du, P., Zheng, S., Li, X., Song, C., Li, R., et al. (2020). Broad and differential animal angiotensin-converting enzyme 2 receptor usage by SARS-CoV-2. J. Virol. *94*, e00940–00920.

Zhou, J., Otter, J.A., Price, J.R., Cimpeanu, C., Garcia, D.M., Kinross, J., Boshier, P.R., Mason, S., Bolt, F., Holmes, A.H., et al. (2020). Investigating SARS-CoV-2 surface and air contamination in an acute healthcare setting during the peak of the COVID-19 pandemic in London. Clin. Infect. Dis. *73*, e1870–e1877.

STAR★METHODS

KEY RESOURCES TABLE

REAGENT or RESOURCE	SOURCE	IDENTIFIER
Antibodies		
Anti-SARS-CoV-2 nucleocapsid protein	Sino Biological	40143-R019 RRID: AB_2827973
Sheep anti-rabbit IgG HRP	Sigma	AP510P
Bacterial and virus strains		
SARS-CoV-2 England/2/2020	Isolated from patient (Davidson et al., 2020)	N/A
SARS-CoV-2/England/IC19/2020	Isolated from patient (McKay et al., 2020)	N/A
SARS-CoV-2/hu/DK/CL-5/1	Isolated from patient (Lassaunière et al., 2021)	N/A
rgSARS-CoV-2 D614G	This paper	N/A
rgSARS-CoV-2 D614G+Y453F	This paper	N/A
Biological samples		
REACT2 convalescent health care worker serum panels	(Moshe et al., 2021)	N/A
Sera from BNT162b2 vaccinated healthcare workers	(Prendecki et al., 2021)	N/.A
Air–liquid interface human airway epithelium (Mucilair)	Epithelix	Mucilair
Chemicals, peptides, and recombinant proteins		
Ribo m7G Cap Analogue	Promega	P1711
TMB substrate	Europa Bioproducts	MO701A
reporter lysis buffer	Promega	E4030
Coelenterazine-H	Promega	S2011
Critical commercial assays		
Ribomax T7 RNA transcription Kit	Promega	P1320
MessengerMax lipofection kit	Thermo	LMRNA001
QIAsymphony DSP Virus/Pathogen Mini Kit	Qiagen	937055
AgPath RT-PCR kit	Life Technologies	AM1005
QuikChange Lightning Multi Site-Directed Mutagenesis Kit	Agilent	97066-324
Luciferase Assay System	Promega	E1500
TransIT-X2	Mirus Bio	MIR 6003
Lipofectamine 3000	Life Technologies	L3000001
Bright-Glo substrate	Promega	E2610
KOD polymerase	Sigma-Aldrich	71086
TURBO-free Kit	Invitrogen	AM1907
$LiCl_2$-based Yeast transformation kit	Merck	YEAST1-1KT
superscript IV reverse transcriptase	Invitrogen	18090010
Deposited data		
Raw sequence reads (Mutations that adapt SARS-CoV-2 to mustelid hosts do not increase fitness in the human airway.)	NCBI BioProject database	BioProject ID PRJNA779209
Experimental models: Cell lines		
African green monkey kidney cells (Vero)	Nuvonis Technologies	N/A
Vero E6 cells	ATCC	ATCC CRL-1586

(*Continued on next page*)

Continued

REAGENT or RESOURCE	SOURCE	IDENTIFIER
Human embryonic kidney cells (293T)	ATCC	ATCC CRL-11268
Baby hamster kidney cells (BHK-21)	ATCC	ATCC CCL-10
Stably transduced ACE2-expressing 293T cells	(Peacock et al., 2021a)	N/A
293Ts stably expressing rLuc-GFP 1-7 effector cells	(Ishikawa et al., 2012)	N/A
BHK-21 target cells stably expressing rLuC-GFP-8-11	(Ishikawa et al., 2012)	N/A
Saccharomyces cerevisiae strain TYC1	(Gaida et al., 2011)	N/A
BHK-hACE2-N	(Rihn et al., 2021)	N/A
Experimental models: Organisms/strains		
Outbred Female Ferrets	Highgate Farms	N/A
Oligonucleotides		
random primer mix	NEB	S1330S
ARTIC Primer set V3	ARTIC Network	N/A
E gene forward primer: ACAGGTA CGTTAATAGTTAATAGCGT	(Zhou et al., 2020)	N/A
E gene reverse primer: ATATTG CAGCAGTACGCACACA	(Zhou et al., 2020)	N/A
Recombinant DNA		
Plasmid: SARS-CoV-2 Spike (and derivatives)	(McKay et al., 2020); This paper	N/A
Plasmid: pCAGGs-GAG-POL	(Peacock et al., 2021a)	N/A
Plasmid: pCSFLW	(Peacock et al., 2021a)	N/A
Plasmid: pDisplay ACE2 (various)	(Conceicao et al., 2020)	N/A
pUC57-Kan	Bio Basic Canada Inc	N/A
pEB2	(Gaida et al., 2011)	N/A
Software and algorithms		
Artic-ncov2019 pipeline v1.2.1	ARTIC Network	N/A
DiversiTools	http://josephhughes.github.io/btctools/	N/A
MAFFT v7.475	(Katoh and Standley, 2013)	N/A
Pangolin COVID-19 Lineage Assigner	(Rambaut et al., 2020a)	N/A
RAxML v8.0.0	(Stamatakis, 2014)	N/A
R *ggtree* package	(Yu et al., 2017)	N/A

RESOURCE AVAILABILITY

Lead contact

Further information and requests for resources and reagents should be directed to and will be fulfilled by the lead contact, Wendy Barclay (w.barclay@imperial.ac.uk).

Materials availability

Novel plasmids generated in this study are available upon request to the lead contact without restriction (for academic research) or with a completed Materials Transfer Agreement (for commercial work).

Data and code availability

Raw sequencing reads have been deposited to the NCBI SRA and are publicly available as of the date of publication. Accession numbers for the associated Bioproject are listed in the key resources table.

This paper does not report original code.

Any additional information required to reanalyze the data reported in this paper is available from the lead contact upon request.

EXPERIMENTAL MODEL AND SUBJECT DETAILS

Ferrets (Mustela putorius furo)

All ferret studies were performed in a containment level 3 laboratory, using a bespoke isolator system (Bell Isolation Systems). Outbred female ferrets (16–20 weeks old) weighing 750–1,000 g were used. Animal research was carried out under a United Kingdom Home Office License, P48DAD9B4.

Cells

African green monkey kidney cells (Vero; Nuvonis Technologies) were maintained in OptiPRO SFM (Life Tech) containing 2x GlutaMAX (Gibco). Human embryonic kidney cells (293T; ATCC; ATCC CRL-11268) were maintained in Dulbecco's modified Eagle's medium (DMEM; Gibco), 10% fetal calf serum (FCS), 1x non-essential amino acids (NEAA; Gibco), 1x penicillin-streptomycin (P/S; Gibco). Stably transduced ACE2-expressing 293T cells were produced as previously described (Peacock et al., 2021a; Rebendenne et al., 2021), and maintained with the addition of 1 μg ml−1 puromycin to growth medium. Baby hamster kidney cells (BHK-21; ATCC CCL-10) were maintained in DMEM (Sigma-Aldrich) supplemented with 10% FCS, 1 mM sodium pyruvate solution (Sigma-Aldrich, Germany), and 1x P/S. Air–liquid interface human airway epithelium (HAEs) cells were purchased from Epithelix and maintained in Mucilair cell culture medium (Epithelix). All cell lines were maintained at 37°C, 5% CO_2. Cell lines were not tested for mycoplasma contamination.

METHOD DETAILS

Biosafety and ethics statement

All laboratory work was approved by the local genetic manipulation safety committee of Imperial College London, St. Mary's Campus (center number GM77), and the Health and Safety Executive of the United Kingdom, under reference CBA1.77.20.1. SARS-CoV-2 reverse genetics work was performed at CVR University of Glasgow under HSE GM notification number is GM223/20.1a. Animal research was carried out under a United Kingdom Home Office License, P48DAD9B4.

Healthcare workers convalescent antisera samples from the REACT2 studies were taken in concordance with the World Medical Association's Declaration of Helsinki. Ethical approval was approved by the South Central-Berkshire B Research Ethic Committee (REC ref: 20/SC/0206; IRAS 283805). Sera from BNT162b2 vaccinated healthcare workers (Prendecki et al., 2021) were collected as part of a study approved by the Health Research Authority (REC ref: 20/WA/0123).

Viruses, reverse genetics, and growth kinetics

The early SARS-CoV-2 strain, England/2/2020 (VE6-T) was previously isolated by Public Health England as previously described (Davidson et al., 2020). The D614G containing strain, SARS-CoV-2/England/IC19/2020, was used as previously described (McKay et al., 2020). The Cluster 5 isolate - SARS-CoV-2/hu/DK/CL-5/1 – was isolated as previously described (Lassaunière et al., 2021) and was kindly provided by Kevin Bewley at Public Health England. All viral stocks used in this study were grown in Vero cells in OptiPRO SFM containing 2x GlutaMAX. Virus titration was performed by median tissue culture infectious dose ($TCID_{50}$) on Vero cells as described previously (Peacock et al., 2021a).

Virus growth kinetics and competition assays were performed as described previously (Brown et al., 2021; Peacock et al., 2021a). Briefly, in air-liquid interface HAEs, before infection cells were washed with serum-free media to remove mucus and debris. Cells were infected with 200 μL of virus-containing serum-free DMEM and incubated at 37°C for 1 h. Inoculum was then removed and cells were washed twice. Time points were taken by adding 200 μL of serum-free DMEM and incubating for 10 mins and 37°C before removal and titration.

Transformation-Associated Recombination (TAR) method in yeast was used to generate the mutant viruses described in this study. We followed essentially previously described methods (Thi Nhu Thao et al., 2020) with some modifications. Briefly, a set of overlapping cDNA fragments representing the entire genome of SARS-CoV-2 Wuhan isolate (GenBank: MN908947.3) were chemically synthesized and cloned into pUC57-Kan (Bio Basic Canada Inc). Where appropriate the relevant synthetic cDNA fragment carried the mutation D614G or Y453F + D614G in the viral S gene. The cDNA fragment representing the 5' terminus of the viral genome contained the bacteriophage T7 RNA polymerase promoter preceded by a short sequence stretch homologous to the *Xho*I-cut end of the TAR in yeast vector pEB2 (Gaida et al., 2011). The fragment representing the 3' terminus contained the T7 RNA polymerase termination sequences followed by a short segment homologous to the *Bam*HI-cut end of pEB2. These cDNA fragments were excised by restriction digestion and gel-extracted or PCR-amplified using appropriate primers. These fragments were then pooled and co-transformed with *Xho*I-*Bam*HI-cut pEB2 into the *Saccharomyces cerevisiae* strain TYC1 (MATa, ura3-52, leu2Δ1, cyh2^r, containing a knockout of DNA Ligase 4) (Gaida et al., 2011) that had been made competent for DNA uptake using the $LiCl_2$-based Yeast transformation kit (YEAST1-1KT; Merck). The transformed cells were plated on minimal synthetic defined (SD) agar medium lacking uracil (Ura) but containing 0.002% (w/v) cycloheximide to prevent selection of cells carrying the empty vector. Following incubation at 30°C for 4 to 5 days, colonies of the yeast transformants were screened by PCR using specific primers to identify those carrying plasmid with fully assembled genomes. Selected positive colonies were then expanded to grow in 200 ml SD-Ura dropout medium and the plasmid extracted as described by Thao et al. (2020)(Thi Nhu Thao et al., 2020). Approximately 4 μg of the extracted material was then

used as template to *in vitro* synthesized viral genomic RNA transcripts using the Ribomax T7 RNA transcription Kit (Promega) and Ribo m7G Cap Analogue (Promega) as per the manufacturer's protocol. Approximately 2.5 μg of the *in vitro* synthesized RNA was used to transfect ~6 x10^5 BHK-hACE2-N cells stably expressing the SARS-CoV-2 N and the human ACE2 genes (Rihn et al., 2021) using the MessengerMax lipofection kit (Thermo Scientific) as per the manufacturer's instructions. Cells were then incubated until signs of viral replication (syncytia formation) became visible (usually after 2-3 days), at which time the medium was collected (P0 stock) and used further as a source of rescued virus to infect VERO E6 cells to generate P1 and P2 stocks. Full genome sequences of viruses collected from P0 and P1 stocks were obtained in order to confirm the presence of the desired mutations and exclude the presence of other spurious mutations. Viruses were sequenced using Oxford Nanopore as previously described (da Silva Filipe et al., 2021).

E gene RT-qPCR

Virus genomes were quantified by E gene RT-qPCR as previously described (Zhou et al., 2020). Viral RNA was extracted from supernatants of swab material using the QIAsymphony DSP Virus/Pathogen Mini Kit on the QIAsymphony instrument (Qiagen). RT-qPCR was then performed using the AgPath RT-PCR (Life Technologies) kit on a QuantStudio™ 7 Flex Real-Time PCR System with the primers specific for SARS-CoV-2 E gene (Corman et al., 2020). For absolutely quantification of E gene RNA copies, a standard curve was generated using dilutions viral RNA of known copy number. E gene copies per ml of original virus supernatant were then calculated using this standard curve.

Live virus neutralisation

Convalescent antisera from health care workers who had tested positive by RT-qPCR were taken from the REACT2 study as described previously (Flower et al., 2020; Moshe et al., 2021). Double dose BNT162b2 (Pfizer-BioNtech) antisera from health care workers was generated as previously described (Prendecki et al., 2021).

Live virus neutralisation assays were performed in Vero cells as described elsewhere (Brown et al., 2021). Briefly serial dilutions of sera were incubated with 100 $TCID_{50}$ of virus for 1 h at room temperature then transferred to 96 well plates of Vero cells. Plates were incubated at 37°C, 5% CO_2 for 42 h before fixing cells in 4% paraformaldehyde (PFA). Cells were permeabilised in methanol 0.6% H_2O_2 and stained for 1 h with an antibody against SARS-CoV-2 nucleocapsid protein (Sino Biological; 40143-R019, 1:300 dilution). Cells were further stained with the secondary antibody sheep anti-rabbit IgG HRP conjugate (Sigma; 1:3000 dilution) for 1 h. TMB substrate (Europa Bioproducts) was added and developed for 20 mins before halting the reaction with 1M HCl. Plates were read at 450 nm and 620 nm and the concentration of serum needed to reduce virus signal by 50% was calculated to give NT50 values.

For the CPE-based neutralisation assay (reverse genetics virus vs Pfizer antisera), serial dilutions of sera were incubated with 100 $TCID_{50}$ of virus for 1 h at 37°C, 5% CO_2 in 96 well plates before a suspension of Vero-ACE2-TMPRSS2 cells were added and incubated for 3 days at 37°C, 5% CO_2. Wells were stained using crystal violet, scored for the presence of virus-induced cytopathic effect and the reciprocal of the highest serum dilution at which protection was seen was calculated as the serum titre.

Plasmids and cloning

Lentiviral packaging constructs pCSLW and pCAGGs-GAGPOL were made as previously described. Mutant SARS-CoV-2 expression plasmids were generated by site-directed mutagenesis using the QuikChange Lightning Multi Site-Directed Mutagenesis Kit (Agilent). Unless otherwise stated all SARS-CoV-2 spike expression plasmids were based on the Wuhan-hu-1 reference sequence (McKay et al., 2020), with the additional substitutions D614G and K1255*STOP (aka the Δ19 mutation or cytoplasmic tail truncation). Animal ACE2 proteins in pDisplay were generated and used as previously described (Conceicao et al., 2020).

Pseudovirus assays

SARS-CoV-2 spike-bearing lentiviral pseudotypes (PV) were generated as described previously (Conceicao et al., 2020; Peacock et al., 2021a). At ICL, 100 mm dishes of 293Ts were transfected using lipofectamine 3000 (Thermo) with a mixture of pCSFLW, pCAGGS-GAGPOL and spike proteins expressed in pcDNA3.1. After 24 h supernatant was discarded and replaced. Pseudovirus-containing supernatant was collected and pooled at 48 and 72 h post-transfection, passed through a 0.45 μm filter, aliquoted, and frozen at -80°C. At the Pirbright Institute pseudovirus was generated in 6-well plates. Cells were transfected using polyethyleneimine (PEI) with a mixture of pCSFLW, p8.91 and SARS-CoV-2 spikes expressed in pcDNA3.1. As before supernatant was discarded and replaced at 24 h post-transfection then harvested and pooled at 48 and 72h. Supernatant was clarified by low-speed centrifugation, aliquoted, and frozen at -80°C.

Pseudovirus assays at ICL were performed as previously described (Peacock et al., 2021a). Briefly 10 mm diameter dishes of 293T cells were transfected with 1 μg of ACE2 of empty vector using lipofectamine 3000. 24 h later cells media was replaced, and cells were resuspended by scraping and plated into 96 well plates and overlayed with pseudovirus. 48 h later cells were lysed with reporter lysis buffer (Promega) and assays were read on a FLUOstar Omega plate reader (BMF Labtech) using the Luciferase Assay System (Promega).

At Pirbright assays were performed largely as previously described (Conceicao et al., 2020). Briefly, BHK-21 cells were transfected with 500 ng of ACE2 or empty vector (pDISPLAY) using TransIT-X2 (Mirus Bio) according to the manufacturer's recommendation. 24 h later, media was removed, and cells were harvested following the addition of 2mM EDTA in PBS, resuspended in DMEM

and plated into white-bottomed 96 wells plates (Corning). Cell were overlayed with pseudovirus 24 h later and incubated for 48 h. Firefly luciferase was quantified whereby media was replaced with 50 μL Bright-Glo substrate (Promega) diluted 1:2 with PBS and read on a GloMax Multi+ Detection System (Promega). CSV files were exported onto a USB flash drive for analysis.

Pseudovirus neutralization assays were performed by incubating serial dilutions of heat-inactivated human convalescent antisera with a set amount of pseudovirus. Antisera/pseudovirus mix was then incubated at 37°C for 1 h then overlayed into 96 well plates of 293T-ACE2 cells. Assays were then lysed and read as described above.

Cell-cell fusion assay

Cell-cell fusion assays were performed as described elsewhere (Conceicao et al., 2020; Thakur et al., 2021). Briefly, 293Ts stably expressing rLuc-GFP 1-7 effector cells (Ishikawa et al., 2012) were transfected with empty vector, WT or mutant SARS-CoV-2 spike proteins. BHK-21 target cells stably expressing rLuC-GFP-8-11 (target cells) were co-transfected with ACE2 expression constructs. Target cells were co-cultured with effector cells 24 h post-transfection and quantification of cell-cell fusion was performed 24 h later with the *Renilla* luciferase substrate, Coelenterazine-H (Promega). Luminescence was read on a Glomax Multi+ Detection System (Promega). CSV files were exported on a USB flash drive for analysis.

Ferret infection study

Ferret (*Mustela putorius furo*) infection studies with SARS-CoV-2 virus were performed as described previously (Peacock et al., 2021a). All ferret studies were performed in a containment level 3 laboratory, using a bespoke isolator system (Bell Isolation Systems). Outbred female ferrets (16–20 weeks old) weighing 750–1,000 g were used. Four donor ferrets were inoculated intranasally with 200 μl of 10^5 p.f.u. of each virus while lightly anaesthetized with ketamine (22 mg kg^{-1}) and xylazine (0.9 mg kg^{-1}).

Prior to the start of the study ferrets were confirmed to be seronegative to SARS-CoV-2. All animals were nasal-washed daily, while conscious, by instilling 2 ml of PBS into the nostrils; the expectorate was collected into disposable 250-ml sample pots. Ferrets were weighed daily post infection, and body temperature was measured daily via subcutaneous IPTT-300 transponder (Plexx B.V).

RNA extraction and sequencing

For Sanger sequencing, RNA was extracted from nasal washes using QIAamp viral RNA mini kit (Qiagen). RNA was reverse transcribed using Superscript IV (Invitrogen) and PCR of the spike was performed using KOD polymerase (Merck). For next generation sequencing RNA from virus-containing samples were extracted using the QIAsymphony DSP Virus/Pathogen mini kit (Qiagen). RNA was DNase-treated using the TURBO-free Kit (Invitrogen; (AM1907). cDNA was synthesized using the superscript IV reverse transcriptase (Invitrogen) and random primer mix (NEB) before amplification by the ARTIC Network protocol using the multiplexed primer scheme version 3. Fast5 files were basecalled with guppy (v.5.0.7) with high accuracy calling (hac). The fastq files produced by Nanopore sequencing were filtered with lengths 400 and 700 using Artic-ncov2019 pipeline v1.2.1 (https://artic.network/ncov-2019/ncov2019-bioinformatics-sop.html) by "artic guppyplex" function. The other function of "artic minion" in the Artic-ncov2019 pipeline with "–medaka –medaka-model r941_min_high_g360 –normalise 0" parameters was then used to process the filtered fastq files to generate ARTIC V3 primer trimmed bam files and consensus genome sequences. These primer trimmed bam files were further analysed using DiversiTools (http://josephhughes.github.io/btctools/) with the "-orfs" function to generate the ratio of amino acid change in the reads and coverage at each site of protein in comparison to the reference SARS-CoV-2 genome (MN908947.3) as we previous description (Dong et al., 2020).

Phylogenetic analysis

All sequences with host species labelled as *Neovison vison* were retrieved from the Global Initiative on Sharing All Influenza Data (GISAID) database (sequences retrieved on 7 July 2021). A table of accession IDs and acknowledgement is given in Table S1. A sequence with only 397 nucleotides (hCoV-19/mink/Spain/NV-2105/2021, EPI_ISL_1490748) was excluded from analysis. Sequences were aligned to the Wuhan-Hu-1 reference genome sequence (MN908947) (Wu et al., 2020) using MAFFT v7.475 (Katoh and Standley, 2013) and the alignment was then checked manually. Seven further sequences were excluded from further analysis as they lacked nucleotide data enabling the determination of amino acid identity at spike positions 453, 486, 501 or 614 (hCoV-19/mink/USA/MI-CDC-II1O-7265/2020, EPI_ISL_925307; hCoV-19/mink/USA/MI-CDC-IHWB-7153/2020, EPI_ISL_925308; hCoV-19/mink/USA/WI-CDC-CX2X-2436/2020, EPI_ISL_1014948; hCoV-19/mink/Netherlands/NB-EMC-3-5/2020, EPI_ISL_523094; hCoV-19/mink/Netherlands/NB-EMC-3-4/2020, EPI_ISL_523093; hCoV-19/mink/Netherlands/NB-EMC-40-4/2020, EPI_ISL_577788; hCoV-19/mink/Denmark/mDK-56/2020, EPI_ISL_641448). Epidemiological lineages were determined using the Pangolin COVID-19 Lineage Assigner(O'Toole et al., 2021; Rambaut et al., 2020a) (pangolin v3.1.5, pangoLEARN v15/06/2021). Phylogenetic analysis was performed using the remaining 936 mink genomes rooted on the Wuhan-Hu-1 reference genome (MN908947) with a general time reversible model of nucleotide substitution, a proportion of invariant sites estimated from the data and a gamma distribution describing among-site rate variation (GTR + I + Γ) built using RAxML v8.0.0 (Stamatakis, 2014) with the phylogeny rooted on the sequence of the virus Wuhan-Hu-1. The maximum likelihood phylogeny was plotted, alongside data on sampling location extracted from the virus name and amino acid identity at spike positions 453, 486, 501 and 614, in R using the *ggtree* package (Yu et al., 2017).

QUANTIFICATION AND STATISTICAL ANALYSIS

Statistics throughout this study were performed using one-way analysis of variance (ANOVA) or Student's t-test and are described in the figure legends. No statistical method was used to predetermine sample size. Several genome sequences were manually removed from the phylogenetic analysis and were described in the associated sections. The experiments were not randomized, and the investigators were not blinded to allocation during experiments and outcome assessment.